Journal of GeoEngineering, Vol. 18, No. 2, pp. 083-092, June 2023
http://dx.doi.org/10.6310/jog.202306_18(2).4

INVESTIGATIONS OF EARTHQUAKE-INDUCED ROCK LANDSLIDE BASED ON THE HOEK-BROWN FAILURE CRITERION

An-Jui Li [1], Chi Hsiao [2], Wei-Chien Wang [3*], Zhi-Guang Qian [4]

ABSTRACT

Slope instability and subsequent landslides can be caused by earthquakes, rainfall, and human activities. For the past several decades, landslides have always been a critical issue in protecting infrastructure. This study investigates rock slope stability by considering the effects of rock mass disturbance based on the Hoek-Brown failure criterion. All of the analyses are conducted using RS2 version 9.0. The Daguangbao landslide caused by the Wenchuan earthquake is adopted as the case study. Various methods accessed widely for slope stability problems with respect to earthquakes are used in this study to determine the possible onset of a landslide. These include the traditional Newmark displacement method, enhanced Newmark method, and time-history dynamic analysis. Nonetheless, it was still found difficult to determine the precise time at which a landslide will occur. However, a reasonable failure mechanism can be obtained as long as the rock mass disturbance on the slope can be evaluated properly.

Key words: Finite element method, newmark method, dynamic analysis, pseudo-static.

1. INTRODUCTION

Slope stability is a conventional geotechnical problem. In recent year, landslides have drawn more and more attention because climate change and rising temperatures are likely to trigger more landslides (Gariano and Guzzetti 2016). In fact, slope instability and resultant landslides can cause significant disasters that jeopardize human lives and lead to property losses. Many factors can induce landslides. These influencing factors include original geometry, geological condition, slope mass properties, rainfall, earthquake, and human activities, among which earthquakes are known to be one of the major causes of landslides (Dong *et al.* 2009; Wu and Chen 2009; Wu *et al.* 2009; Bozzano *et al.* 2011; Hung *et al.* 2018; Candia *et al.* 2019; Wu and Hsieh 2021). In practice, in addition to evaluating the impact of the earthquake on slope stability according to design specifications, it is also important to effectively capture the initial time of slope failure. The onset time provides an understanding of the failure mechanism and progressive behavior of the earthquake-induced landslide. Moreover, It is also an important reference for slope remediation (Lin *et al.* 2017; Hung *et al.* 2018).

Nowadays, the primary methods to evaluate earthquake-induced slope failure include the pseudo-static analysis (Newmark 1965; Dong *et al.* 2009; Wu and Chen 2008, 2009; Wu and Tsai 2011) and time-dependent dynamic analysis (Wu 2010; Wu *et al.* 2017; Hung *et al.* 2018; Wu and Hsieh 2021). According to Newmark method (Newmark 1965), two modified Newmark sliding models were proposed (Wu and Chen 2008, 2009; Wu and Tsai 2011) to evaluate the dynamic back-calculation of the shear strength parameters of the sliding surfaces for the Chiu-fen-erh-shan and Tsaoling landslides. The new dynamic back-calculation procedure they proposed is especially suitable in case of unavailable groundwater monitoring data. Additionally, the Finite element method (FEM), discontinuous deformation analysis (DDA), and 3D distinct element methods (3DEC) are useful and common time-dependent dynamic analyses to simulate earthquake-induced slope failure. The discrete element method (DDA) was adopted by Wu *et al.* (2009) to simulate failure progression for Tsaoling landslide. Wu (2010) used three available algorithms to incorporate seismic impacts into DDA simulations for earthquake-induced slope failure. The study showed it is incorrect to evaluate absolute movements of falling/sliding and base blocks by applying time-dependent accelerations to falling/sliding blocks. In addition, the case of the Daguangbao rock avalanche is considered to demonstrate the capability of the new geometric restriction to solve the mechanism that causes unwanted base block distortion in a seismic DDA (Wu *et al.* 2017). Wu and Hsieh (2021) adopted 3DEC numerical program to investigate the debris movement and deposition of the Chiu-fen-erh-shan landslide under the impact of the Chi-Chi earthquake (Wu and Hsieh 2021). The result showed that the essential 3D characteristics of the landslide and a post-failure configuration were captured by 3DEC and were similar to that observed in the field.

To evaluate slope stability, geotechnical engineers employ the factor of safety (FS) to determine whether the slope is stable or not. In slope stability assessments, the material strength parameters must be considered carefully. In general, a reasonable numerical tool and failure criterion can be selected to perform a slope stability analysis. Practically, the conventional Mohr-Coulomb failure criterion is still used commonly to address rock mass problems (Rutqvist *et al.* 2009; Latha and Garaga 2010; Song *et al.* 2011; Fan *et al.* 2013; Zhao *et al.* 2014). As indicated by Li *et al.* (2008), using the Mohr-Coulomb failure criterion can overestimate the FS for rock slopes, particularly steep slopes, and theoretically, applying the Hoek-Brown failure criterion directly to assess

Manuscript received October 21, 2022; revised May 4, 2023; accepted May 19, 2023.
[1] Associate Professor, Department of Civil and Construction Engineering, National Taiwan University of Science and Technology, Taipei 106, Taiwan.
[2] Former student, Department of Civil and Construction Engineering, National Taiwan University of Science and Technology, Taipei 106, Taiwan.
[3*] Ph.D. (corresponding author), Department of Civil and Construction Engineering, National Taiwan University of Science and Technology, Taipei 106, Taiwan (e-mail: d10305001@mail.ntust.edu.tw).
[4] Ph.D., School of Engineering, Deakin University, VIC 3217, Australia.

rock slope stability can obtain more accurate results. In addition, Hoek and Karzulovic (2000) emphasized that rock mass disturbance can vary with depth in a rock slope. Previous investigations (Qian *et al.* 2017; Li *et al.* 2019; Li *et al.* 2020) have also demonstrated that considering rock mass disturbance variance in a slope is reasonable.

As mentioned previously, earthquake effects are essential considerations in slope stability assessments in earthquake-prone regions. Therefore, it is important to have a better understanding of a rock slope behavior and reaction during an earthquake. A literature review showed that a number of slopes have been investigated over the past several decades with the Mohr-Coulomb parameters using time-history analyses (Hung *et al.* 2018; Luo *et al.* 2019). With consideration that the rock mass disturbance decreases with depth, a landslide on the Daguangbao slope is adopted and investigated in this study based on the latest version of the Hoek-Brown failure criterion.

2. METHODOLOGY

2.1 The Generalized Hoek-Brown Failure Criterion

In general, most slope analyses use the Mohr-Coulomb failure criterion to input soil parameters (c' and ϕ'), and ignore the non-linear nature of the rock mass failure envelope. In addition, the non-linearity is more pronounced at the low confining stresses that operate in slope stability problems. Merifield *et al.* (2006) mentioned that the Hoek-Brown failure criterion is one of the few non-linear criteria used by practicing engineers to estimate rock mass strength. Therefore, this failure criterion is adopted in the study.

In Hoek *et al.* (2002), the latest version of the Hoek-Brown criterion is expressed as:

$$\sigma_1' = \sigma_3' + \sigma_{ci}\left(m_b \frac{\sigma_3'}{\sigma_{ci}} + s \right)^a \tag{1}$$

where

$$m_b = m_i \exp\left(\frac{\mathrm{GSI}-100}{28-14D} \right) \tag{2}$$

$$s = \exp\left(\frac{\mathrm{GSI}-100}{9-3D} \right) \tag{3}$$

$$a = \frac{1}{2} + \frac{1}{6}\left(e^{-GSI}/15 - e^{-20}/3 \right) \tag{4}$$

$$E_m(\mathrm{GPa}) = \left(1-\frac{D}{2}\right)\sqrt{\frac{\sigma_{ci}}{100}} \times 10^{\left(\frac{\mathrm{GSI}-10}{40}\right)} \tag{5}$$

$$E_m(\mathrm{GPa}) = \left(1-\frac{D}{2}\right) \times 10^{\left(\frac{\mathrm{GSI}-10}{40}\right)} \tag{6}$$

The rock mass modulus of deformation is given by Eq. (5), which applies for $\sigma_{ci} \leq 100$ MPa. For $\sigma_{ci} > 100$ MPa, use Eq. (6). E_m is Young's Modulus, and s and a rely on the geological strength index (GSI), which describes the rock mass quality, and σ_{ci} and m_i represent the intact uniaxial compressive strength and material constant, respectively. The parameter D is a factor that depends on the degree of disturbance and ranges between 0 and 1. Hoek *et al.* (2002) introduced the disturbance factor (D) to deal with rock mass disturbance, and the range of D is between 0 (for undisturbed rock masses) and 1 (for disturbed rock masses). In fact, the disturbance factor (D) has a significant effect on the evaluation of a rock mass slope's stability. Equations (7) and (8) are used to obtain the equivalent Mohr-Coulomb parameters (Qian *et al.* 2017; Chen and Lin 2019; Li *et al.* 2019).

$$c' = \frac{\sigma_{ci}\left[(1+2\alpha)\, s + (1-\alpha)\, m_b\, \sigma_{3n}' \right](s + m_b\, \sigma_{3n}')^{\alpha-1}}{(1+\alpha)(2+\alpha)\sqrt{1+\left(6\alpha\, m_b\,(s+m_b\,\sigma_{3n}')^{\alpha-1}\right)/\,(1+\alpha)(2+\alpha)}} \tag{7}$$

$$\varphi' = \sin^{-1}\left[\frac{6\alpha\, m_b\,(s+m_b\,\sigma_{3n}')^{\alpha-1}}{2(1+\alpha)(2+\alpha)+6\alpha\, m_b\,(s+m_b\,\sigma_{3n}')^{\alpha-1}} \right] \tag{8}$$

where $\sigma_{3n} = \sigma_{3\max}'/\sigma_{ci}$.

$$\frac{\sigma_{3\max}'}{\sigma_{cm}'} = 0.72\left[\frac{\sigma_{cm}'}{\gamma H} \right]^{-0.91} \tag{9}$$

$$\sigma_{cm}' = \sigma_{ci}\frac{\left(m_b + 4s - \alpha(m_b - 8s)\right)(m_b/4+s)^{\alpha-1}}{2(1+\alpha)(2+\alpha)} \tag{10}$$

In this study, several different approaches are employed to analyze the Daguangbao landslide during the Wenchuan earthquake. These include the pseudo-static analysis and time-history analysis using the finite element method. The results obtained from the pseudo-static method are used in the Newmark method to obtain the slope movement. The purpose of this study was to explore the different methods to analyze the possible time of the rock landslide onset.

2.2 Finite Element Method

In this study, the finite element software, RS2 9.0, was used to perform a time-history dynamic analysis (Rocscience 2019). RS2 9.0 is a two-dimensional finite element method software that can be applied to soil and rock masses. The software includes a wide range of engineering applications, for example, slope stability, excavation design, and groundwater seepage and dynamic analyses. One of its features is the use of the shear strength reduction method (Tschuchnigg *et al.* 2015a, 2015b; Liu *et al.* 2018). Various failure criteria can be applied, such as the Mohr-Coulomb and Hoek-Brown failure criteria.

The concept of the finite element method is to divide the object into small elements, and observe their interaction. The method divides the continuum or physical model into a grid structure where the elements are connected. The deformation or displacement within the element is approximated by the node displacement interpolation function. An external force is exerted on the node, and the discretization equation of the continuum composed of the node action effect and the reaction relation is solved for the governing equation under the known external force to obtain each node's displacement along the continuum.

In setting the dynamic boundary, this study refers to the RS2 manual (Rocscience 2019), which suggests that the transmit condition is set on the lateral boundary, and the absorb condition on the bottom boundary. In the dynamic response analysis, the material damping is repeated by the shear strain effect within the material, and friction loss causes energy loss. Therefore, the energy is not preserved during the wave transmission process. In this study, RS2 9.0 uses Rayleigh damping, which is calculated with Eq. (11):

$$C = \alpha \mathbf{M} + \beta \mathbf{K} \tag{11}$$

where α is the mass damping coefficient, **M** is the mass matrix, β is the stiffness damping coefficient, and **K** is the stiffness matrix.

In fact, it is difficult to determine the exact damping ratio for a given slope. Generally speaking, rock materials' energy consumption may be less obvious than that of soil materials. Because the seismic wave energy propagates faster in rock than in soil, rock materials' damping ratio should be smaller than that of soil materials. Based on the case of Las Colinas slope (Koltuk and Fernandez-Steeger 2014), the preliminary study was conducted to verify the rationality of the damping ratio setting. When the damping ratio is 3%, the analysis results are reasonable and almost consistent with the Koltuk and Fernandez-Steeger's study. In this study, the Daguangbao slope is composed of broken rock materials. Therefore, the extended range of damping ratios (3%, 5%, and 10%) is adopted to compare the effect on slope failure mechanism. The maximum shear plastic strain is used in RS2 as a reference for the shape of the failure surface.

2.3 Newmark Method

Newmark proposed a method to analyze slope displacement in 1965 (Newmark 1965). The concept is that a slope will deform only if the safety factor (FS) obtained from pseudo-static analysis is smaller than 1. The critical acceleration (a_{tc}) is defined as a horizontal acceleration leads to FS = 1. The sequence of an earthquake strong-motion record that exceed the critical horizontal acceleration is integrated twice to obtain the cumulative displacement of the slope. The Newmark sliding block analysis was used to evaluate the safety of earth-rock dams after earthquakes in early years. This analysis can calculate displacements of slopes during earthquakes. The cumulative displacement is often used to evaluate slope stability after an earthquake. Two Newmark methods are used in this study. The first is the traditional Newmark displacement method, and the other is the enhanced Newmark method.

2.4 Traditional Newmark Displacement Method

The traditional Newmark displacement method largely simplifies the slope as a block on an inclined plane, and calculates the block's displacement after an earthquake. The basic assumptions of the theory of this analysis are as follows (Romeo 2000):

(1) The sliding block is a rigid-plastic body and acts on a sliding surface with little cohesion;

(2) The block will move when the seismic acceleration exceeds the sliding body's critical acceleration (a_{tc}). On the other hand, if the seismic acceleration is lower than the critical acceleration, no displacement will occur;

(3) The critical acceleration (a_{tc}) does not depend on the displacement, but plastic deformation is allowed on the sliding surface.

(4) The material static and dynamic strength are the same. This analysis does not consider the excess pore water pressure the earthquake causes, so it does not consider the liquefaction behavior.

The surface acceleration that exceeds the critical acceleration will cause permanent displacement of the block on the slope. The critical acceleration (a_{tc}) can be defined in Eq. (12):

$$a_{tc} = (\mathrm{FS} - 1)\, \mathrm{g} \sin \delta \tag{12}$$

2.5 Enhanced Newmark Method

Huang *et al.* (2001) accounted for the horizontal and vertical motions with an analysis referred to as the enhanced Newmark method. Equations (13) to (15) can convert the original seismic wave's acceleration in the east-west, north-south, and vertical directions into the horizontal acceleration, a_d, and the vertical acceleration, a_n, on the slope, and the acceleration along the slope, a_s:

$$a_d = a_E \cos \delta \cos \phi_s - a_N \cos \delta \sin \phi_s - a_V \sin \delta \tag{13}$$

$$a_s = a_E \sin \phi_s - a_N \cos \phi_s \tag{14}$$

$$a_n = a_E \sin \delta \cos \phi_s - a_N \sin \delta \sin \phi_s - a_V \sin \delta \tag{15}$$

Among them, a_E, a_N, and a_V are the accelerations in the east-west, north-south, and vertical directions, respectively, ϕ_s is the angle between the slope direction and north, and δ is the slope inclination. The description above shows that the sliding surface is considered a plane. Therefore, the inputs required in Eqs. (13)-(15) should be determined approximately if the slope failure surface is not a plane failure. According to the concept of force balance, when the sum of the frictional force and cohesion on the inclined plane is greater than the glide driving force, the force normal to the slope is mg cos δ, where m is the mass of the free-body, g is the gravitational acceleration, and δ is the dip angle. A friction force, μ_s mg cos δ, balances the mg sinδ downhill force gravity generates. This is $m(\mathrm{g} \sin \delta - a_d) \le \mu_s\, m(\mathrm{g} \cos \delta + a_n) + cA$, where μ_s, c and A are the friction coefficient, cohesion, and contact area, respectively. It can be seen that the Mohr-Coulomb strength parameters are still needed when using Eqs. (13)-(15).

In the enhanced Newmark method, the block is in a stable state; otherwise, it will accelerate and move. The down-dip sliding acceleration, S, can be calculated as shown in Eq. (16). By integrating the acceleration duration curve of part $S > 0$ twice, the permanent displacement can be obtained. If the vertical acceleration is not considered ($a_n = 0$), Eq. (16) can be represented by Eq. (17). As Huang *et al.* (2001) indicated, Eq. (17) can be seen as the input used in the traditional Newmark displacement method. As Eqs. (16) and (17) show, the Mohr-Coulomb strength parameters are still required as inputs.

$$S = (\mathrm{g} \sin \delta - a_d) - \mu_s (\mathrm{g} \cos \delta + a_n) - \frac{cA}{m} \tag{16}$$

$$S1 = (\mathrm{g} \sin \delta - a_d) - \mu_s (\mathrm{g} \cos \delta) - \frac{cA}{m} \tag{17}$$

2.6 Case Study: Daguangbao Landslide

The 2008 Wenchuan earthquake triggered tens of thousands of landslides, among which the Daguangbao landslide was the

largest. It was estimated that this landslide affected an area of 73 thousand to 10 million square meters, or a total volume of earthwork of approximately 1.051 billion cubic meters (Huang *et al.* 2008; Chigira *et al.* 2010). The landslide is located on a cantilever wall only 6.5 kilometers from the Yingxiu-Beichuan fault zone. It traveled approximately 4.5 kilometers, blocked the Huangdongzi Valley, and is nearly 600 meters high. The terrain in the landslide area before the earthquake showed that the elevation decreased from west to east (Zhang *et al.* 2013, 2015). The highest peak elevation of Daguangbao before the slide failure is at an altitude of 3047 m and the lowest is at an altitude of 1,450 m where it is at the bottom of Huangdongzi Valley. The landslide's terrain can be divided into three parts along the main sliding direction (Huang *et al.* 2008; Zhang *et al.* 2013, 2015). The geological profile before the earthquake shown in Fig. 1 can be divided into three parts. The first is Daguangbao peak, where the height of the ridge ranges from 3047 to 2700 meters, and the slope angle is between 55° and 60°. The second part is the middle of the slope, where the average slope angle is 30°, and the altitude difference is 1000 meters, from 2700 to 1700 meters. The third part ranges from 2000 to 1500 meters, and the slope angle is 50° to 55°. In this study, the seismic acceleration from 51JYH station (31.8°N, 104.6°E) is adopted, approximately 35 kilometers away from the landslide (Wen *et al.* 2010).

The simplified material parameters of the Daguangbao slope model in this study are obtained from Zhang *et al.* (2013), as shown in Tables 1 and 2. It is worth noting that they used the equivalent Mohr-Coulomb parameters for the analysis. However, the Hoek-Brown strength parameters directly are used to perform pseudo-static and time-history analyses with FEM in this study. Based on pseudo-static analyses, the critical horizontal acceleration (kh_{cr}) is obtained, and then cumulative displacement of the slope is calculated using Newmark method. According to some previous studies (Zhang *et al.* 2013, 2015; Wu *et al.* 2017, *etc.*), the dip direction of the slope profile adopted in this study is N60°E. Then the input acceleration is the combination of the east-west and north-south accelerations using Eq. (18) to form a 60° north-east direction (N60°E), as shown in Fig. 2(a). In time-history analysis, the combined horizontal acceleration is added to the bottom of the model. The vertical acceleration, shown in Fig. 2(b), is only considered in the Enhanced Newmark method.

$$a_{N60E} = a_{E\text{-}W} \times \sin 60° + a_{N\text{-}S} \times \cos 60° \quad (18)$$

As mentioned previously, the Daguangbao slope is composed of three materials, as shown in Fig. 1. In this study, the slope is investigated by considering two different rock mass profiles, referred to as Scenarios 1 and 2. The descriptions of the scenarios and the differences in the rock masses in the slope are introduced separately.

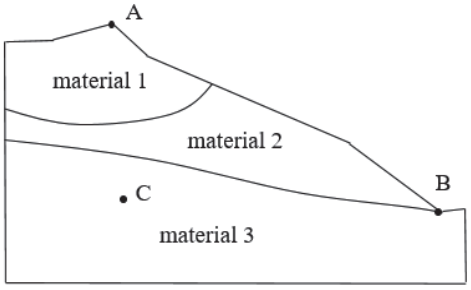

Fig. 1 Rock mass profile for Scenario 1

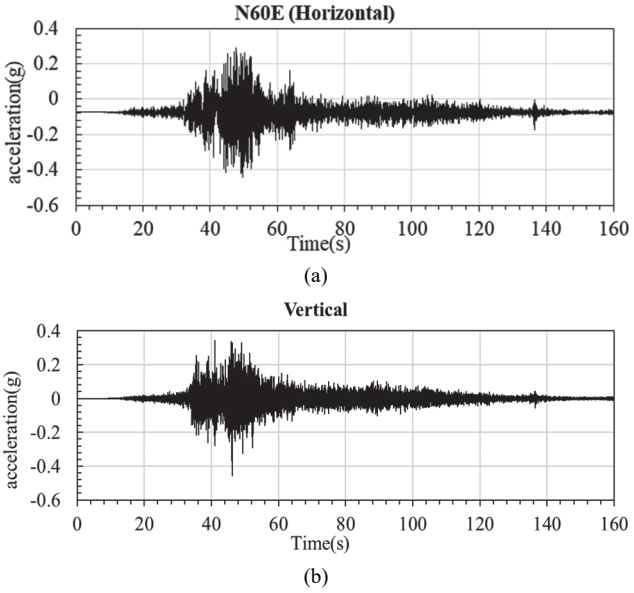

Fig. 2 51JYH station-acceleration data. (a) N60°E horizontal acceleration; (b) Vertical acceleration

Scenario 1

Figure 1 shows the rock mass profile for Scenario 1. The information on the size of each material is based on the Daguangbao slope's original appearance Huang *et al.* (2012) presented. As mentioned previously, the simplified rock mass parameters are shown in Tables 1 and 2.

Table 1 Daguangbao slope model input parameters

	σ_{ci} (MPa)	GSI	m_i	D
Material 1	43.8	40	12	1
Material 2	87.2	40	9	1
Material 3	87.2	70	7	1

Table 2 Daguanagbao slope material parameters

	Material 1	Material 2	Material 3
Unit weight of rock, γ (kN/m^3)	25	26	26
Elastic modulus E (GPa)	1.86	2.63	14.76
Poisson's ratio	0.2	0.2	0.1

Scenario 2

According to Hoek and Karzulovic (2000), it would be inappropriate to assign a constant disturbance factor to a rock slope. In fact, the disturbance factor (D) has a significant effect on the evaluation of a rock mass slope stability. Li *et al.* (2019) followed the study of Hoek and Karzulovic (2000). It was demonstrated that the disturbed region for this rock slope is about one slope height perpendicular to the slope surface. In addition, the disturbance factor (D) decreases with depth linearly, and thus the Daguangbao slope failure mechanism can be simulated reasonably. It should be noted that Zhang *et al.* (2015) did not account for the fact that the rock mass disturbance varies with depth. In their study, D = 1 was set for the entire slope. This explains why the failure surface does not agree well with the surface observed. Therefore, Zhang *et al.* (2015) adjusted the rock slope material profile. Based on the above

descriptions and assumptions, as shown in Fig. 3 and Table 3, the disturbance factor (D = 1-0.415, from the top surface to bottom) in Scenario 2 decreases linearly with slope depth. This consideration is similar to that Li *et al.* (2019) adopted. In addition, Young's Modulus is also changed accordingly.

3. RESULTS AND DISCUSSION

3.1 Results of Traditional Newmark Displacement Method

Using the pseudo-static method, a critical horizontal acceleration (kh_{cr}) of 0.05g was obtained under Scenario 1. Based on the combined horizontal acceleration (N60°E) and kh_{cr}, the slope displacement could be calculated by the traditional Newmark displacement method, as shown in Fig. 4. From previous studies (California Geological Survey 2008; Miles and Keefer 2009; Jibson2011), when the slope displacement reaches 5-10 cm during the earthquake, it may represent the time when the slope begins to fail and the landslide begins. In this study, the lower bound value (5 cm) is defined as threshold displacement to evaluate the beginning failure time of the slope. The results from the traditional Newmark displacement method can be seen in Fig. 4, where the displacement reached 5 cm at approximately the 43rd to 44th seconds, and the maximum displacement value was 33.88 cm. It can be estimated that the time at which the Daguangbao slope might have begun to fail was at approximately the 43rd second after the earthquake's onset.

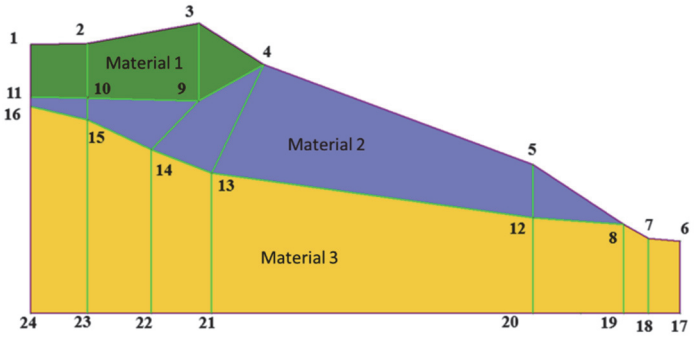

Fig. 3 Rock mass profile and consideration of disturbance factor for Scenario 2

Table 3 Disturbance factor for Scenario 2

Point	Disturbance (D)	Point	Disturbance (D)
1	1	13	0.778
2	1	14	0.745
3	1	15	0.847
4	1	16	0.877
5	1	17	0.82
6	1	18	0.85
7	1	19	0.82
8	1	20	0.7
9	0.895	21	0.493
10	0.892	22	0.415
11	0.895	23	0.457
12	0.895	24	0.46

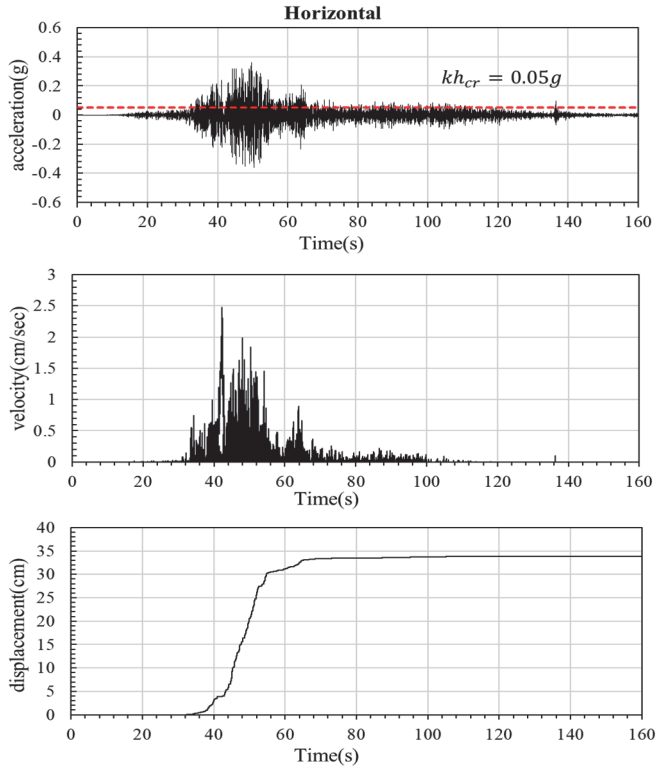

Fig. 4 Scenario 1 results - traditional Newmark displacement method

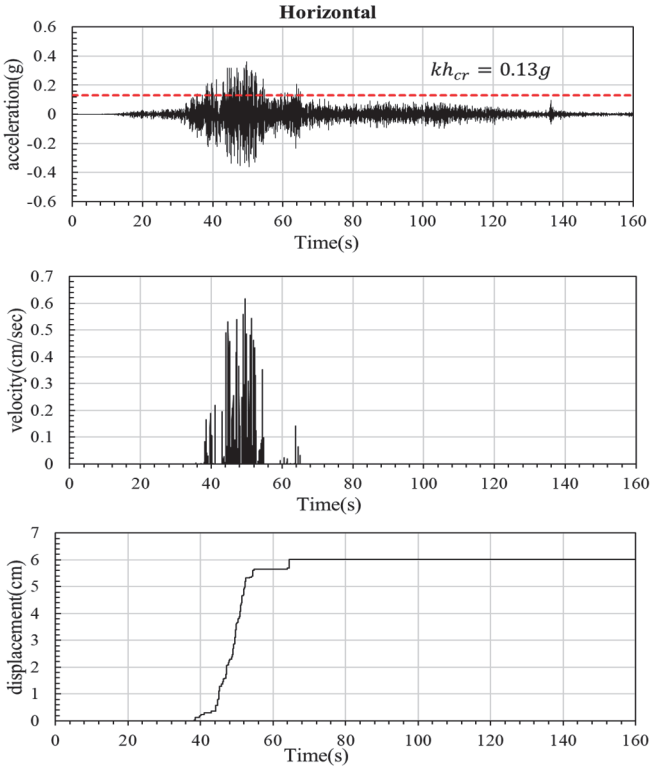

Fig. 5 Scenario 2 results - traditional Newmark displacement method

The pseudo-static method is also adopted to obtain the critical horizontal acceleration (kh_{cr}) of 0.13g under Scenario 2, as shown in Fig. 5. kh_{cr} = 0.13g agreed with the result in Li *et al.* (2020) where kh_{cr} = 0.12g was obtained. In addition, the displacement reached 5 cm at approximately the 52nd to 53rd seconds, and the maximum displacement value was 6.01 cm. Thus, the estimated time at which the Daguangbao slope failed may have been at the 52nd second. From the results obtained above, the magnitudes of kh_{cr} differed because the rock mass profiles differed. Hence, the maximum displacement obtained and the approximated slope failure time differ. In fact, it is reasonable for the slope displacement to increase when kh_{cr} decreases. The maximum displacements obtained for the different scenarios are summarized in Table 4.

3.2 Results from the Enhanced Newmark Method

The enhanced Newmark method used here considers both the vertical and horizontal acceleration along the sliding surface, S, in Eq. (16). Figures 6 and 7 show the displacements calculated for the three different scenarios. As mentioned previously, the enhanced Newmark method still requires the Mohr-Coulomb strength parameters to calculate the displacement. Therefore, the equivalent inputs, c' and ϕ', from Eqs. (7) and (8) are also included in Figs. 6 and 7. It should be noted that the magnitudes of c' and ϕ' are means because the failure surfaces pass through different materials. Hung *et al.* (2018) evaluated the possible slope failure time and landslide onset using $S > 0$. Based on the same consideration, the slope failure time of 40 second can be estimated for Scenarios 1. In addition, the acceleration that accounted only for horizontal acceleration along the sliding surface, $S1$ in Eq. (17), was also investigated. As shown in Table 4, considering the vertical acceleration along the sliding surface can increase the slope displacement. However, the increment was insignificant for this earthquake event. This trend was consistent with the finding in Zhang *et al.* (2013).

3.3 Results from FEM-Based Time-History Analyses

According to some studies (Wei and Cheng 2009; Tschuchnigg *et al.* 2015; Lin *et al.* 2020; Li *et al.* 2022, *etc.*), the maximum shear plastic strain is employed to determine the slope failure surface in this study. The slope displacement in Scenario 2 in FEM was shown in Fig. 8 where the points monitored can be referred to Fig. 1. It should be noted that, the displacements were only slightly changed when the vertical acceleration is considered. In addition, the failure surface is nearly unchanged, which is consistent with the result of Zhang *et al.* (2013). Figure 8 shows that the displacement decreases with increasing damping ratio. It is worth noting that the critical displacement of 5 cm is also used in FEM to determine the failure time. Although various damping ratios are adopted in this study, they had no significant effects on the determinations of the failure surface and failure time. Therefore, in the

Table 4 Daguangbao slope model input parameters

	Traditional Newmark displacement method	Enhanced Newmark method (S)	Enhanced Newmark method ($S1$)	kh_{cr} by traditional Newmark displacement method	a_{ec} by enhanced Newmark method
Scenario 1	33.88 cm	3.412 cm	3.283 cm	0.05 g	0.172 g
Scenario 2	6.01 cm	0.517 cm	0.425 cm	0.13 g	0.247 g

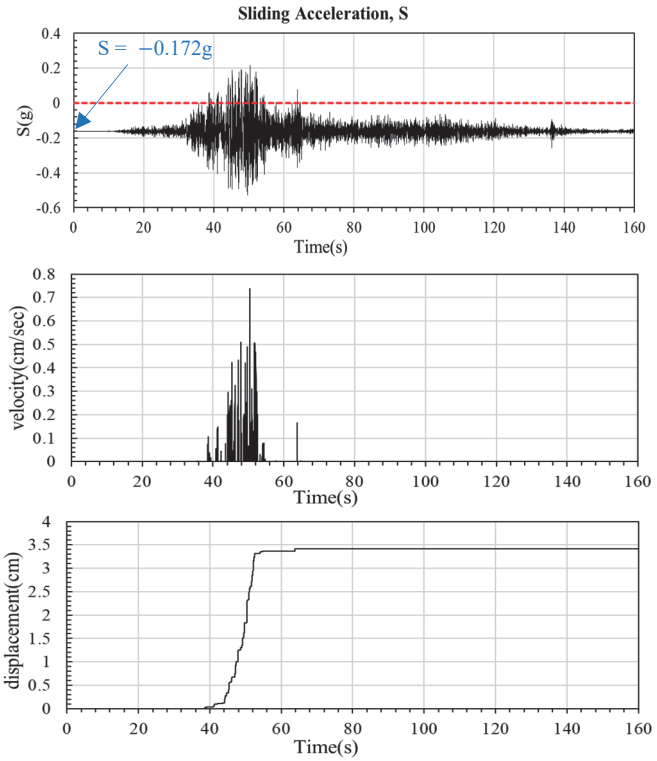

Fig. 6 Scenario 1 - enhanced Newmark method (c' = 1.523 MPa and ϕ' = 10.81°)

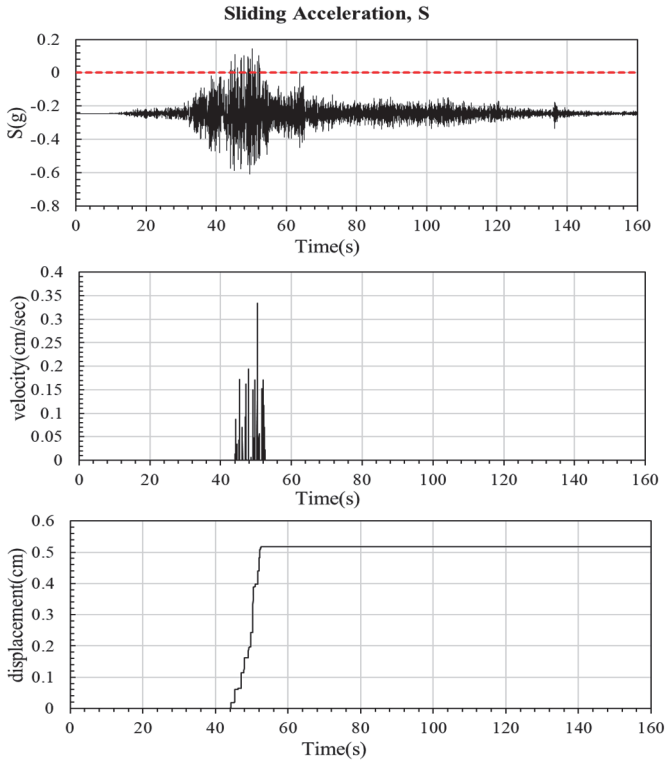

Fig. 7 Scenario 2 - enhanced Newmark method (c' = 1.849 MPa and ϕ' = 12.60°)

following discussion, the results are based primarily on the 3% damping ratio. When horizontal acceleration (N60°E) is input, by observing the development of the maximum shear plastic strain and 5 cm displacement, the possible time at which the slope failed was the 40th second. As shown in Fig. 9, the failure surface developed for the upper slope is slightly larger than that reported by Fan *et al.* (2017) and Cui *et al.* (2018). However, they are still reasonably similar. It should be highlighted that the maximum shear plastic strains in Figs. 9 and 10 are nearly the same as those obtained from the pseudo-static analyses.

Figure 10 shows the failure surface considering a 5 cm displacement for Scenario 2 when the slope failure time is at the 43rd second. The entire slope failure shape is also reasonable when comparing to that reported by Fan *et al.* (2017) and Cui *et al.* (2018). Figures 9 and 10 likely demonstrated that a 5 cm displacement is reasonable to capture the slope failure mechanism. Based on the FEM time-history analysis results, the failure surfaces can be identified. Both Scenario 1 and Scenario 2 provide reasonable failure surfaces. In fact, the rock mass profile employed in Scenario 2 considered that the rock mass disturbance decreases with depth. Therefore, the maximum shear plastic zone for the upper slope in Fig. 10(b) matched the observed sliding surface slightly better than that in Fig. 9(b). It implied that considering the disturbance factor change in a slope is probably essential to obtain a better failure surface in a numerical analysis.

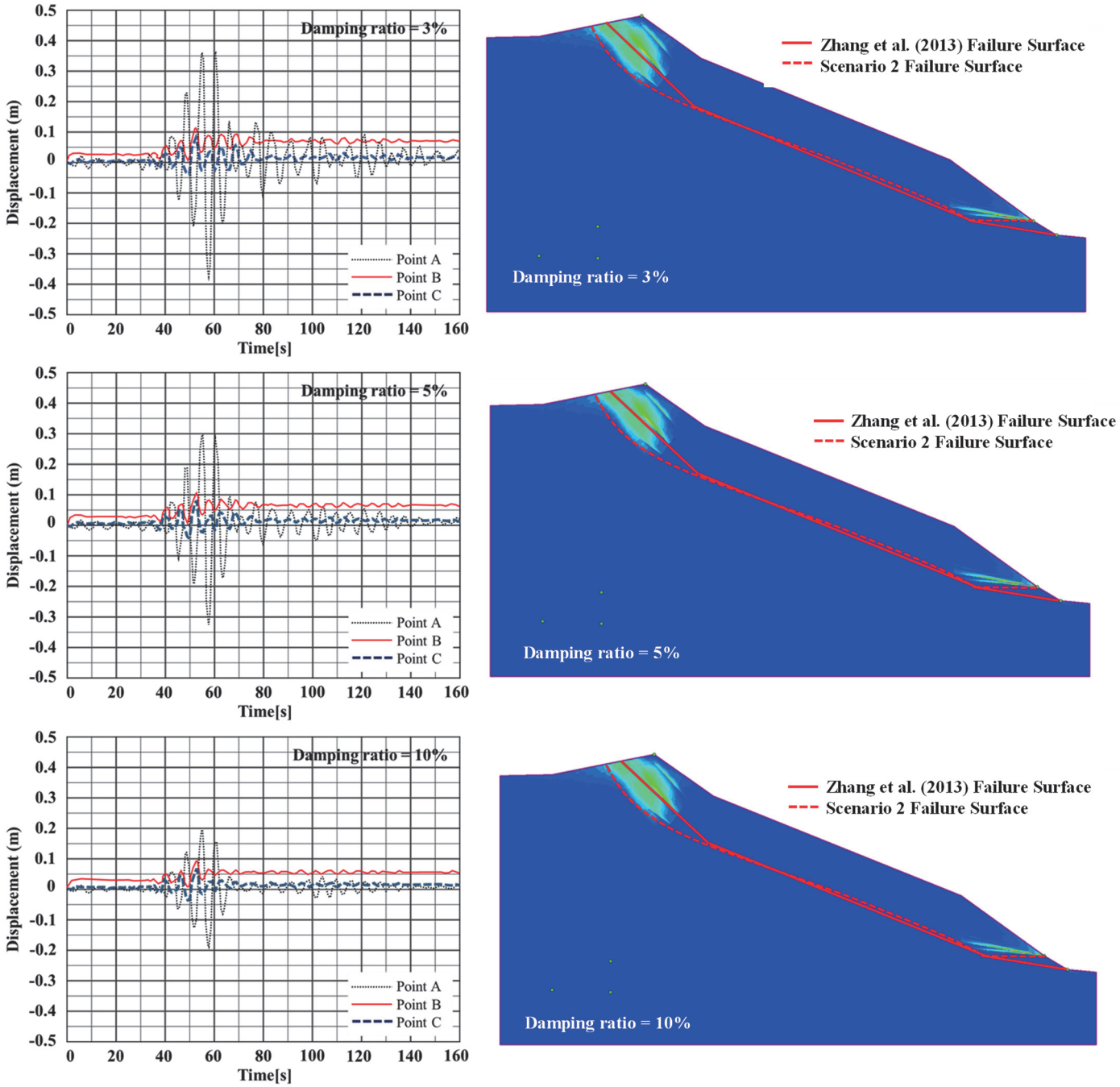

Fig 8 Slope displacement and failure surface in Scenario 2 for different damping ratios (only horizontal acceleration)

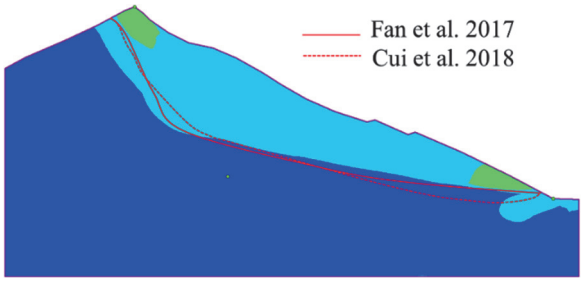

(a) Displacement

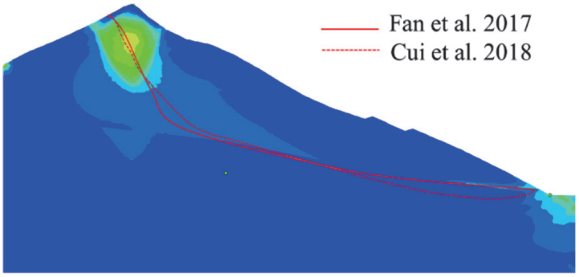

(a) Displacement

Fig. 9 Scenario 1 failure surface by FEM at 40th second

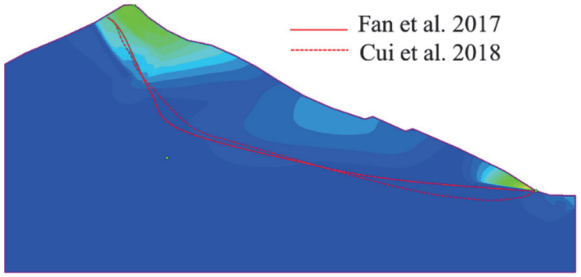

(b) Maximum shear plastic strain

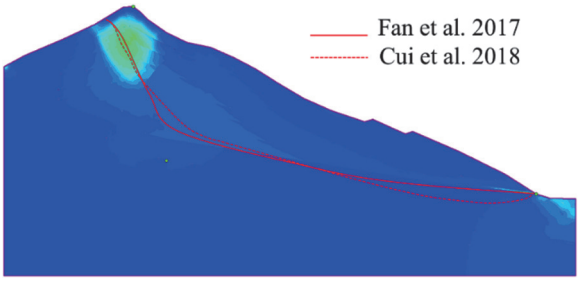

(b) Maximum shear plastic strain

Fig. 10 Scenario 2 failure surface by FEM at 43rd second

4. COMPARISONS OF DIFFERENT METHODS

Table 4 shows that the displacement with the enhanced Newmark method is much smaller than that with the traditional Newmark displacement method. Further, the result obtained in this study differs from that in Huang *et al.* (2001), in which the displacement with the traditional Newmark displacement method was smaller. The reason is that these two methods are based on different theories and considerations of vertical acceleration. For the traditional Newmark displacement method, the displacement is calculated by considering critical horizontal acceleration (kh_{cr}), while the vertical acceleration is not considered. However, in the enhanced Newmark method, the displacement is calculated based on critical acceleration (a_{ec}) derived by the force equilibrium considering vertical acceleration. Therefore, a more detailed comparison between these two approaches is made.

It is known that the kh_{cr} value can control the displacement obtained with the traditional Newmark displacement method significantly. Therefore, the authors focus on observing the acceleration, S, in the enhanced Newmark method. It is found that the displacements are integrated and obtained based on different starting points between these two methods. In the traditional Newmark displacement method, kh_{cr} (critical horizontal acceleration) from the pseudo-static method is adopted. However, using the enhanced Newmark method would likely provide a different critical acceleration (a_{ec}), as shown in Table 4. In Lin (2017), the critical acceleration (a_{ec}) = $-S$ was defined when time = 0. In Fig. 6 for Scenario 1, a_{ec} = 0.172g can be obtained. A similar approach is used to find the a_{ec} values for Scenario 2. It should be noted that a_{ec} in the enhanced Newmark method considers the vertical acceleration effect, but kh_{cr} in the traditional Newmark displacement method does not adopt it. Table 4 shows that a_{ec} in the enhanced Newmark method is greater than kh_{cr} in the traditional Newmark displacement method. Although the definitions of a_{ec} and kh_{cr} are not exactly the same, they have a certain relation that still makes the comparison meaningful.

In addition, S is calculated using Eqs. (13)-(15) where the equivalent Mohr-Coulomb parameters are needed, as indicated previously. Li *et al.* (2012) and Qian *et al.* (2017) noted that using the equivalent Mohr-Coulomb parameters could overestimate the FS for rock slopes. This issue might also influence the slope movement evaluation based on the enhanced Newmark method. The discussion above would explain the significant differences in the displacements between the two Newmark methods. On the other hand, it was observed that the change in the slope movement is small when the vertical acceleration for this case study was considered.

From the results, Table 5 shows that the possible slope failure time obtained differs, although the same judgments from previous studies were adopted. It can be seen that the possible slope failure time in Scenario 1 is earlier than that in Scenario 2. It is reasonable because the entire rock masses have less disturbance before the earthquake. As discussed previously, Scenario 2 gave a slightly better sliding surface than Scenario 1. Based on this consideration, the possible failure time is between 43 and 52 seconds. Overall, it is very difficult to determine which method provides a better estimation of the slope failure time, and more case studies and detailed investigations are definitely required.

Table 5 Slope failure time determined by different methods

	Traditional Newmark displacement method	Enhanced Newmark method	FEM
Scenario 1	43rd second	38th second	40th second
Scenario 2	52nd second	44th second	43rd second

5. CONCLUSIONS

This study adopted the Hoek-Brown failure criterion to analyze the Daguangbao landslide caused by the Wenchuan earthquake. The traditional Newmark displacement method, enhanced Newmark method, and FEM time-history dynamic analysis were employed in this study. Based on the FEM time-history analysis

results, both Scenarios 1 and 2 can provide reasonable failure surfaces. In fact, the rock mass profile was adjusted in Scenario 2, which considers that rock mass disturbance decreases with depth. This indicates that considering rock mass disturbance carefully in a slope can help determine a realistic failure mechanism.

The vertical acceleration was found to be insignificant in the estimations of earthquake-induced slope displacements in the Daguangbao landslide. In addition, the displacement calculated with the enhanced Newmark method is much smaller than that with the traditional Newmark displacement method. It was found that the magnitude of the critical acceleration determined with these two approaches could differ greatly, possibly for two reasons. The first is that the two Newmark methods are developed based on different theories, while the other is that the equivalent Mohr-Coulomb strength parameters are used in the enhanced Newmark method, which could overestimate the rock mass strength. Although various methods were employed in this study to determine the potential slope failure time, it remains difficult to capture the precise moment that the landslide occurred. Overall, many factors affect the failure time of the earthquake-induced slope. A failure criterion, threshold displacement, is only adopted in this study, but some influencing factors are not still considered, such as the analyzed motion, topographic effect, etc. Hence, more investigations and cases are needed to study and clarify these influencing factors in determining the potential slope failure time.

FUNDING

The authors received no funding for this work.

DATA AVAILABILITY STATEMENT

The data and/or computer codes used/generated in this study are available from the corresponding author on reasonable request.

CONFLICT OF INTEREST STATEMENT

The authors declare that there is no conflict of interest.

REFERENCES

Bozzano, F., Lenti, L., Martino, S., Montagna, A., and Paciello, A. (2011). "Earthquake triggering of landslides in highly jointed rock masses: Reconstruction of the 1783 Scilla rock avalanche (Italy)." *Geomorphology*, **129**(3-4), 294-308. https://doi.org/10.1016/j.geomorph.2011.02.025

California Geological Survey, California State Mining, and Geology Board. (2008). *Guidelines for Evaluating and Mitigating Seismic Hazards in California*. **117**, California Geological Survey, California Department of Conservation, Sacramento, CA.

Candia, G., Montgomery, J., Lemnitzer, A., and Martínez, A. (2019). "The September 19, 2017 Mw 7.1 Puebla-Mexico City earthquake: Observed rockfall and landslide activity." *Soil Dynamics and Earthquake Engineering*, **130**, 105972. https://doi.org/10.1016/j.soildyn.2019.105972

Cui, S., Pei, X., and Huang, R. (2018). "Effects of geological and tectonic characteristics on the earthquake-triggered Daguangbao landslides, China." *Landslides*, **15**(4), 649-667. https://doi.org/10.1007/s10346-017-0899-3

Chigira, M., Wu, X., Inokuchi, T., and Wang, G.H. (2010). "Landslides induced by the 2008 Wenchuan earthquake, Sichuan, China", *Geomorphology*, **118**(3-4), 225-238. https://doi.org/10.1016/j.geomorph.2010.01.003

Chen, Y. and Lin, H. (2019). "Consistency analysis of Hoek–Brown and equivalent Mohr–coulomb parameters in calculating slope safety factor." *Bulletin of Engineering Geology and the Environment*, **78**, 4349-4361. https://doi.org/10.1007/s10064-018-1418-z

Dong, J.J., Lee, W.R., Lin, M.L., Huang, A.B., and Lee, Y.L. (2009). "Effects of seismic anisotropy and geological characteristics on the kinematics of the neighboring Jiufengershan and Hungtsaiping landslides during Chi-Chi earthquake." *Tectonophysics*, **466**(3-4), 438-457. https://doi.org/10.1016/j.tecto.2007.11.008

Fan, H.B., Lai, J.X., and Hou, D.D. (2013). "The bench method numerical simulation of soft rock tunnel." *Applied Mechanics and Materials*, **438**, 949-953. https://doi.org/10.4028/www.scientific.net/AMM.438-439.949

Fan, X., Xu, Q., Westen, C., Huang, R., and Tang, R. (2017). "Characteristics and classification of landslide dams associated with the 2008 Wenchuan earthquake." *Geoenvironmental Disasters*, **4**(12). https://doi.org/10.1186/s40677-017-0079-8

Gariano, S.L. and Guzzetti, F. (2016). "Landslides in a changing climate." *Earth-Science Reviews*, **162**, 227-252. https://doi.org/10.1016/j.earscirev.2016.08.011

Hoek, E. and Karzulovic, A. (2000). "Rock mass properties for surface mines, in: Hustrulid, W.A., McCarter M.K., van Zyl, D.J.A. (Eds), *Slope Stability in Surface Mining*, Society for Mining, Metallurgical and Exploration (SME), Littleton, CO, 59-70.

Hoek, E., Carranza-Torres, C., and Corkum, B. (2002). "Hoek-Brown failure criterion-2002 edition." *Proceedings of NARMS-Tac.*, **1**(1), 267-273.

Huang, R.Q., Pei, X.J., and Li, T.B. (2008). "Basic characteristics and formation mechanism of the largest scale landslide at Daguangbao occurred during the Wenchuan earthquake." *Journal of Engineering Geology*, **17**(6), 730-741 (in Chinese with English abstract).

Huang, R., Pei, X., Fan, X., Zhang, W., Li, S., and Li, B. (2012). "The characteristics and failure mechanism of the largest landslide triggered by the Wenchuan earthquake, May 12, 2008, China." *Landslides*, **9**(1), 131-142. https://doi.org/10.1007/s10346-011-0276-6

Hung, C., Lin, G.W., Syu, H.S., Chen, C.W., and Yen, H.Y. (2018). "Analysis of the Aso-bridge landslide during the 2016 Kumamoto earthquakes in Japan." *Bulletin of Engineering Geology and the Environment*, **77**(4), 1439-1449. https://doi.org/10.1007/s10064-017-1103-7

Huang, C.C., Lee, Y.H., Liu, H.P., Keefer, D.K., and Jibson, R.W. (2001). "Influence of surface-normal ground acceleration on the initiation of the Jih-Feng-Erh-Shan landslide during the 1999 Chi-Chi, Taiwan, earthquake." *Bulletin of the Seismological Society of America*, **91**(5), 953-958. https://doi.org/10.1785/0120000719

Jibson, R.W. (2011). "Methods for assessing the stability of slopes during earthquakes-A retrospective." *Engineering Geology*, **122**(1-2), 43-50. https://doi.org/10.1016/j.enggeo.2010.09.017

Koltuk, S. and Fernandez-Steeger, T.M., (2014). "Evaluation of seismic stability of coherent landslides: Analytical approach versus FEM." *Proceedings of 5th International INQUA Meeting Conference on Paleoseismology, Active Tectonics and Archeoseismology*, Busan, Korea, **5**, 21-27.

Latha, G.M., and Garaga, A. (2010). "Seismic stability analysis of a Himalayan rock slope." *Rock Mechanics and Rock Engineering*, **43**(6), 831-843. https://doi.org/10.1007/s00603-010-0088-3

Li, A.J., Cassidy M., Wang Y., Merifield R., and Lyamin A.

(2012). "Parametric Monte Carlo studies of rock slopes based on the Hoek-Brown failure criterion." *Computers and Geotechnics*, **45**, 11-18. https://doi.org/10.1016/j.compgeo.2012.05.010

Li, A.J., Merifield, R., and Lyamin, A. (2008). "Stability charts for rock slopes based on the Hoek–Brown failure criterion." *International Journal of Rock Mechanics and Mining Sciences*, **45**(5), 689-700. https://doi.org/10.1016/j.ijrmms.2007.08.010

Li, A.J., Qian, Z., Jiang, J.C., and Lyamin, A. (2019). "Seismic slope stability evaluation considering rock mass disturbance varying in the slope." *KSCE Journal of Civil Engineering*, **23**(3), 1043-1054. https://doi.org/10.1007/s12205-019-0963-8

Li, A.J., Fatty, A., and Yang, I., (2020). "Use of evolutionary computation to improve rock slope back analysis." *Applied Sciences*, **10**(6), 2012. https://doi.org/10.3390/app10062012

Li, A.J., Wang, W.C., and Lin, H.D. (2022). "Investigation of slope reinforcement with drilled shafts in colluvium soils." *Geomechanics and Engineering*, **31**(1), 71-86. https://doi.org/10.12989/gae.2022.31.1.071

Lin, G.W., Hung, C., and Syu, H.S. (2017). "Evaluation of an enhanced FS method for finding the initiation time of earthquake-induced landslides." *Bulletin of Engineering Geology and the Environment*, **78**(1), 497-506. https://doi.org/10.1007/s10064-017-1083-7

Lin, H.D., Wang, W.C., and Li, A.J. (2020). "Investigation of dilatancy angle effects on slope stability using the 3D finite element method strength reduction technique." *Computers and Geotechnics*, **118**(103295). https://doi.org/10.1016/j.compgeo.2019.103295

Liu, Y., Xiao, H., Yao, K., Hu, J., and Wei, H. (2018). "Rock-soil slope stability analysis by two-phase random media and finite elements." *Geoscience Frontiers*, **9**(6), 1649-1655. https://doi.org/10.1016/j.gsf.2017.10.007

Luo, J., Pei, X., Evans, S.G., and Huang, R. (2019). "Mechanics of the earthquake-induced Hongshiyan landslide in the 2014 Mw 6.2 Ludian earthquake, Yunnan, China." *Engineering Geology*, **251**, 197-213. https://doi.org/10.1016/j.enggeo.2018.11.011

Merifield, R.S., Lyamin, A.V., and Sloan, S. (2006). "Limit analysis solutions for the bearing capacity of rock masses using the generalised Hoek–Brown criterion." *International Journal of Rock Mechanics and Mining Sciences*, **43**(6), 920-937. https://doi.org/10.1016/j.ijrmms.2006.02.001

Miles, S.B. and Keefer, D.K. (2009). "Evaluation of CAMEL—comprehensive areal model of earthquake-induced landslides." *Engineering Geology*, **104**(1-2), 1-15. https://doi.org/10.1016/j.enggeo.2008.08.004

Newmark, N.M. (1965). "Effects of earthquakes on dams and embankments." *Geotechnique*, **15**(2), 139-160. https://doi.org/10.1680/geot.1965.15.2.139

Qian, Z., Li, A.J., Lyamin, A., and Wang, C. (2017). "Parametric studies of disturbed rock slope stability based on finite element limit analysis methods." *Computers and Geotechnics*, **81**, 155-166. https://doi.org/10.1016/j.compgeo.2016.08.012

Romeo, R. (2000). "Seismically induced landslide displacements: A predictive model." *Engineering Geology*, **58**(3-4), 337-351. https://doi.org/10.1016/S0013-7952(00)00042-9

Rocscience (2019). *Rocscience RS2 Online Help*. Retrieved from https://www.rocscience.com/help/rs2/#t=getting_started%2FRS2_Applications_Overview.htm

Rocscience (2019). *SLIDE Online Help*. Retrieved from https://www.rocscience.com/help/slide2/#t=getting_started%2FGetting_Started.htm

Rutqvist, J., Börgesson, L., Chijimatsu, M., Hernelind, J., Jing, L., Kobayashi, A., and Nguyen, S. (2009). "Modeling of damage, permeability changes and pressure responses during excavation of the TSX tunnel in granitic rock at URL, Canada." *Engineering Geology*, **57**(6), 1263-1274. https://doi.org/10.1007/s00254-008-1515-6

Song, K.I., Cho, G.C., and Lee, S.W. (2011). "Effects of spatially variable weathered rock properties on tunnel behavior." *Probabilistic Engineering Mechanics*, **26**(3), 413-426. https://doi.org/10.1016/j.probengmech.2010.11.010

Tschuchnigg, F., Schweiger, H., and Sloan, S.W. (2015a). "Slope stability analysis by means of finite element limit analysis and finite element strength reduction techniques. Part I: Numerical studies considering non-associated plasticity." *Computers and Geotechnics*, **70**, 169-177. https://doi.org/10.1016/j.compgeo.2015.06.018

Tschuchnigg, F., Schweiger, H., and Sloan, S.W. (2015b). "Slope stability analysis by means of finite element limit analysis and finite element strength reduction techniques. Part II: Back analyses of a case history." *Computers and Geotechnics*, **70**, 178-189. https://doi.org/10.1016/j.compgeo.2015.07.019

Wei, W.B. and Cheng, Y.M. (2009), "Strength reduction analysis for slope reinforced with one row of piles", *Computers and Geotechnics*, **36**(7), 1176-1185. https://doi.org/10.1016/j.compgeo.2009.05.004

Wen, X.P., Xie, J.J., Gao, M.T., Hu, Y.X., and Chau, K.T. (2010). "Near-Source Strong Ground Motion Characteristics of the 2008 Wenchuan Earthquake." *Bulletin of the Seismological Society of America*, **100**(5B), 2425-2439. https://doi.org/10.1785/0120090266

Wu, J.H. and Tsai, P.H. (2011). "New dynamic procedure for back-calculating the shear strength parameters of large landslides." *Engineering Geology*, **123**(1-2), 129-147. https://doi.org/10.1016/j.enggeo.2011.01.010

Wu, J.H. and Chen, C.H., (2008). "Force-based and Displacement-based Back Analysis of Shear Strengths: Case of Tsaoling Landslide." *Wseas Transactions on Advances in Engineering Education*, **4**(5), 200-209.

Wu, J.H. and Chen, C.H., (2009). "Back calculating the seismic shear strengths of the tsaoling landslide associated with accelerograph and GPS data." *Iranian Journal of Science and Technology, Transaction B: Engineering*, **33**(4), 301-311

Wu, J.H., Lin, J., and Chen, C. (2009). "Dynamic discrete analysis of an earthquake-induced large-scale landslide." *International Journal of Rock Mechanics and Mining Sciences*, **46**(2), 397-407. https://doi.org/10.1016/j.ijrmms.2008.07.010

Wu, J.H. (2010). "Seismic landslide simulations in discontinuous deformation analysis." *Computers and Geotechnics*, **37**(5), 594-601. https://doi.org/10.1016/j.compgeo.2010.03.007

Wu, J.H. and Hsieh, P.H. (2021). "Simulating the post-failure behavior of the seismically-triggered Chiu-fen-erh-shan landslide using 3DEC." *Engineering Geology*, **287**, 106113. https://doi.org/10.1016/j.enggeo.2021.106113

Wu, J.H., Do, T.N., Chen, C.H., and Wang, G.H. (2017). "New geometric restriction for the displacement-constraint points in discontinuous deformation analysis." *International Journal of Geomechanics*, **17**(5), E4016002. https://doi.org/10.1061/(ASCE)GM.1943-5622.0000648

Zhao, K., Janutolo, M., Barla, G., and Chen, G. (2014). "3D simulation of TBM excavation in brittle rock associated with fault zones: The Brenner Exploratory Tunnel case." *Engineering Geology*, **181**, 93-111. https://doi.org/10.1016/j.enggeo.2014.07.002

Zhang, Y., Chen, G., Zheng, L., Li, Y., and Wu, J. (2013). "Effects of near-fault seismic loadings on run-out of large-scale landslide: a case study." *Engineering Geology*, **166**, 216-236. https://doi.org/10.1016/j.enggeo.2013.08.002

Zhang, Y., Zhang, J., Chen, G., Zheng, L., and Li, Y. (2015). "Effects of vertical seismic force on initiation of the Daguangbao landslide induced by the 2008 Wenchuan earthquake." *Soil Dynamics and Earthquake Engineering*, **73**, 91-102. https://doi.org/10.1016/j.soildyn.2014.06.036